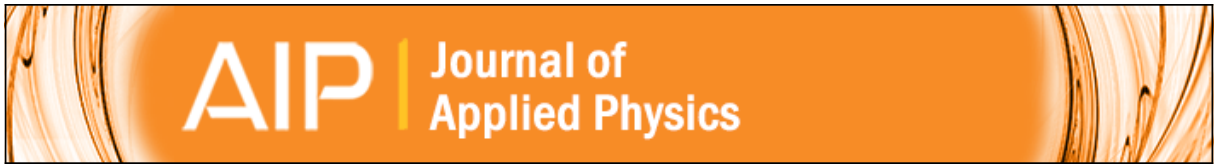

Structural, electrical, and optical analysis of ion implanted semi-insulating InP

C. Carmody, H. H. Tan, C. Jagadish, O. Douhéret, K. Maknys, S. Anand, J. Zou, L. Dao, and M. Gal

Citation: Journal of Applied Physics **95**, 477 (2004); doi: 10.1063/1.1633349
View online: http://dx.doi.org/10.1063/1.1633349
View Table of Contents: http://scitation.aip.org/content/aip/journal/jap/95/2?ver=pdfcov
Published by the AIP Publishing

Structural, electrical, and optical analysis of ion implanted semi-insulating InP

C. Carmody, H. H. Tan, and C. Jagadish[a)]
Department of Electronic Materials Engineering, Research School of Physical Sciences and Engineering, The Australian National University, Canberra, ACT 0200, Australia

O. Douhéret, K. Maknys, and S. Anand[b)]
Department of Microelectronics and Information Technology (IMIT), The Royal Institute of Technology (KTH), ELECTRUM 229, S-16440 KISTA, Sweden

J. Zou
Division of Materials and Centre for Microscopy and Microanalysis, The University of Queensland, QLD 4076, Australia and Australian Key Center for Microscopy & Microanalysis, The University of Sydney, Sydney, NSW, 2006, Australia

L. Dao and M. Gal
School of Physics, The University of New South Wales, Sydney, NSW, 2052, Australia

(Received 24 July 2003; accepted 20 October 2003)

Semi-insulating InP was implanted with MeV P, As, Ga, and In ions, and the resulting evolution of structural properties with increased annealing temperature was analyzed using double crystal x-ray diffractometry and cross sectional transmission electron microscopy. The types of damage identified are correlated with scanning spreading resistance and scanning capacitance measurements, as well as with previously measured Hall effect and time resolved photoluminescence results. We have identified multiple layers of conductivity in the samples which occur due to the nonuniform damage profile of a single implant. Our structural studies have shown that the amount and type of damage caused by implantation does not scale with implant ion atomic mass. © *2004 American Institute of Physics.* [DOI: 10.1063/1.1633349]

I. INTRODUCTION

The interest already displayed in low temperature grown (LT) and ion implanted GaAs, which was found to have ultrashort carrier lifetimes, good mobilities, and high resistivities,[1–5] has been a motivation for similar studies into other semiconductors. Ion implanted InP has a great deal of potential in terms of device applications; because of its short carrier lifetimes, this material could be used in saturable absorbers for the mode locking of solid state lasers, and when p-InP samples are implanted, or Fe^+ is implanted into the semi-insulating material, it is possible to achieve high sheet resistivities in addition to the short lifetimes, and thereby obtain a material which could be used for fabrication of ultrafast photodetectors.[6,7] High resistivity InP has also been investigated through isolation studies.[8–11] Below we present the results from our investigations into the structural, electrical, and optical properties of implanted semi-insulating InP, focusing in particular on how the damage profile can be correlated with profiles of electrical characteristics.

Electrical characterization methods based on scanning probe microscopy have emerged as promising techniques for two-dimensional mapping of electrical properties at the nanometer scale.[12] Application of scanning capacitance microscopy (SCM) and scanning spreading resistance microscopy (SSRM) for characterization of both Si and III–V based materials and devices, has already been reported.[13–16] The obtainable lateral resolution (20–50 nm) is typical of the diameter of a probe tip used in atomic force microscopy (AFM). SCM and SSRM are complementary techniques and very well suited to characterization of electrical properties of ion implanted InP. Particularly, investigation of sample cross-sections provides such information at different locations.

Our results provide extensive information on implanted InP which can help to further the optimizing of implant and annealing conditions for use in devices.

II. EXPERIMENT

Semi-insulating (100) InP samples were implanted at 200 °C with P, As, Ga, and In ions to a dose of 10^{16} cm^{-2}, and at energies of 1, 2, 2.1, and 3.3 MeV, respectively. Transport of ions in matter (TRIM) simulations have predicted that the maximum damage resulting from implantation at these energies will lie approximately 1 μm from the surface. Samples were subsequently annealed at 400, 500, 600, and 700 °C for 30 s. Double crystal x-ray diffractometry (DCXRD) and cross-sectional transmission electron microscopy (XTEM) were then performed on these samples. Hall effect measurements using the van der Pauw method were used to obtain the overall electrical characteristics. Time resolved photoluminescence (TRPL) using a femtosecond self-mode locked Ti:sapphire laser, with a $LiIO_3$ nonlinear crystal, yielded carrier lifetime data. The laser was tunable

a)Electronic address: cxj109@rsphysse.anu.edu.au
b)Electronic address: anand@imit.kth.se

between 750 and 900 nm, the pulse width was 80 fs, the repetition rate 85 MHz, and the output power was 200 mW at $\lambda = 780$ nm.

Scanning capacitance microscopy (SCM) and scanning spreading resistance microscopy (SSRM) were used to obtain electrical characteristics as a function of depth. In this case the samples consisted of undoped InP, about 2 μm thick, grown on n^+ InP substrates, which were then implanted with the different ion species at the energies already listed above. The SCM measurements were carried out with a Digital Instrument Nanoscope Dim 3000 microscope provided with capacitance measurement electronics using commercial Pt-Ir5 coated tips (nanosensors GmBH). The capacitance is measured using a sensor operating at 915 MHz and the tip-sample bias is controlled separately by low-frequency ac and dc voltages. The SSRM measurements were performed with a Digital Instrument Nanoscope Dim 3100 microscope equipped with a SSRM module. Commercial boron-doped diamond coated tips (nanosensors GmBH) were used. The current is measured using a logarithmic amplifier and the dc bias is applied to the sample. For both SCM and SSRM, the sample cross section was obtained by manual cleaving. In the case of SCM, the native oxide formed on the cleaved surface by air exposure served as a thin oxide between the tip and the sample. Cross-sectional TEM (XTEM) samples were prepared by mechanical grinding followed by ion-beam thinning and then examined in a Philips CM 12 operating at 120 kV.

III. RESULTS AND DISCUSSION

A. DCXRD

Figure 1 depicts the evolution of the DCXRD rocking curves as a function of annealing temperature, for all the implanted samples. P and As ion implantation produced similar x-ray spectra—and presumably similar types of damage—with periodic fringes on the negative angle side of the rocking curves. These fringes have been associated with a sharply defined layer of compressive in-plane strain; this damage is mostly annealed out at a temperature of 600 °C, and the rocking curves become similar to that of the unimplanted sample, except for the larger full width at half maximum (FWHM) caused by residual defects in the material. The spectra for Ga implantation also show these periodic fringes, but over a narrower angle range, and they are still present after annealing at 700 °C. Possibly, the implanted Ga atoms are affecting the recrystallization processes during annealing. Implantation with In ions does not yield these fringes at all. Both Ga and In ion implantation also result in broad features at $\theta/2\theta = 600$ arcsec [this did not occur for the P or As case, hence the truncation of the scans at $\theta/2\theta = 200$ arcsec in Figs. 1(a) and 1(b)]. At temperatures above 500 °C, this feature is annealed out.

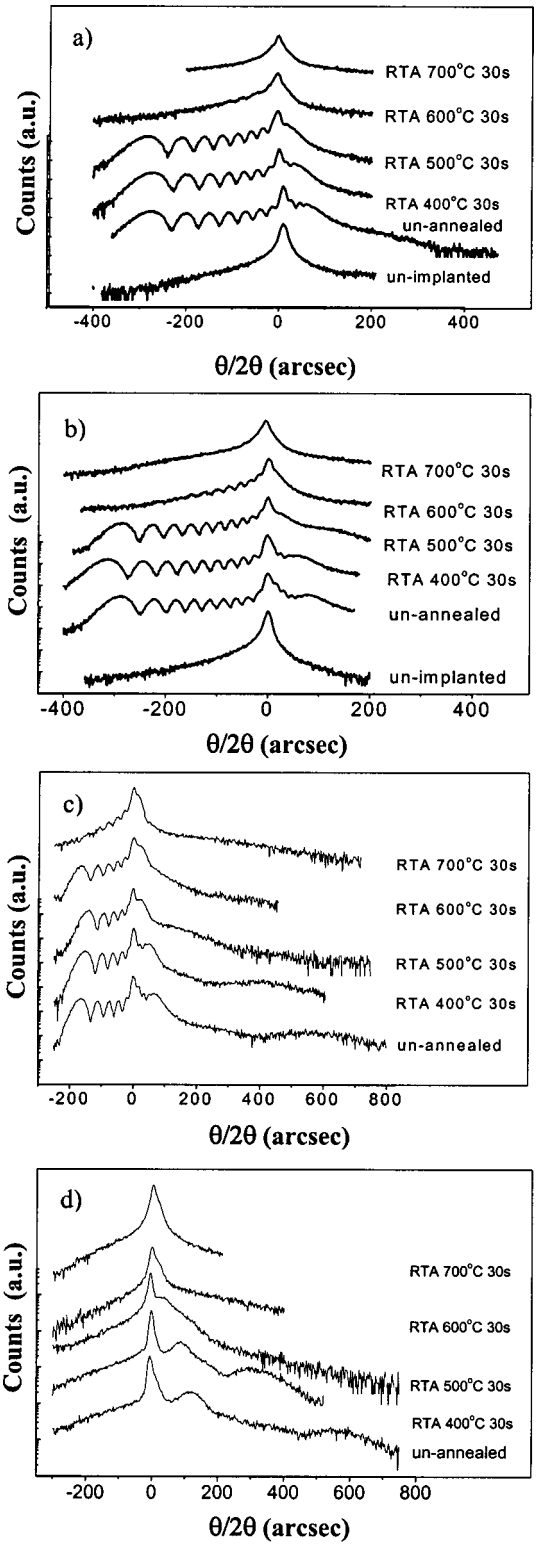

FIG. 1. X-ray rocking curves from InP ion implanted at 200 °C with a dose of 1×10^{16} cm^{-2}. 1 MeV P (a), 2 MeV As (b), 2.1 MeV Ga (c), and 3.3 MeV In (d). Spectra vertically shifted for clarity.

Etching as well as XTEM measurements allow more precise understanding of the depth at which these features in the DCXRD measurements have originated. Figure 2(a) shows x-ray rocking curves for InP implanted with 2 MeV As ions to a dose of 10^{16} cm^{-2}, and then etched with 100% HCl in successive 10 s intervals. Clearly the in-plane tensile strain features close to the substrate peak come from the 0.8 μm nearest the surface, while the periodic in-plane compressive strain structures result from a narrow layer $\sim$1 μm into the sample. Figure 2(b) shows the results for a similar experiment performed on a 10^{16} cm^{-2} In ion implanted sample. These measurements show that the broad features at

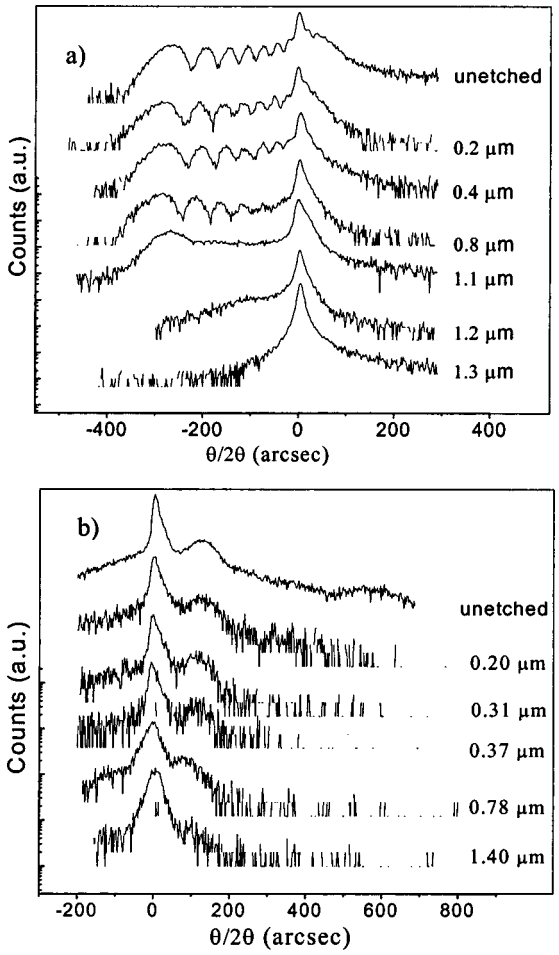

FIG. 2. DCXRD spectra for (a) 2 MeV As and (b) 3.3 MeV In ion implanted InP at 200 °C to a dose of 10^{16} cm^{-2} as a function of etch depth.

large positive angles come from within the first 0.2 μm from the surface, and again that the in-plane tensile strain features closer to the substrate peak are generated in the first 0.8 μm from the surface.

B. XTEM

Cross-sectional transmission electron microscopy provides a kind of visual inspection of the implant-induced defective regions in the samples as a function of depth. Figure 3 shows XTEM diffraction contrast images for the SI InP samples implanted with As, Ga, and In ions, both prior to and after annealing at 700 °C for 30 s. The contrast in the images is due to the strain caused by lattice defects, although point defects or small clusters, which produce only a small amount of strain, are not detectable. A thin layer of damage is visible ~1 μm from the surface in all as-implanted samples, which corresponds to the depth of maximum damage predicted by the TRIM simulations. Adding this information to that already gleaned through DCXRD/etching experiments described above, we conclude that this must be the region responsible for the periodic fringes seen in the DCXRD experiments. Annealing causes the visible damage to ''spread'' vertically. This phenomenon suggests that the majority of lattice defects in the as-implanted samples are in

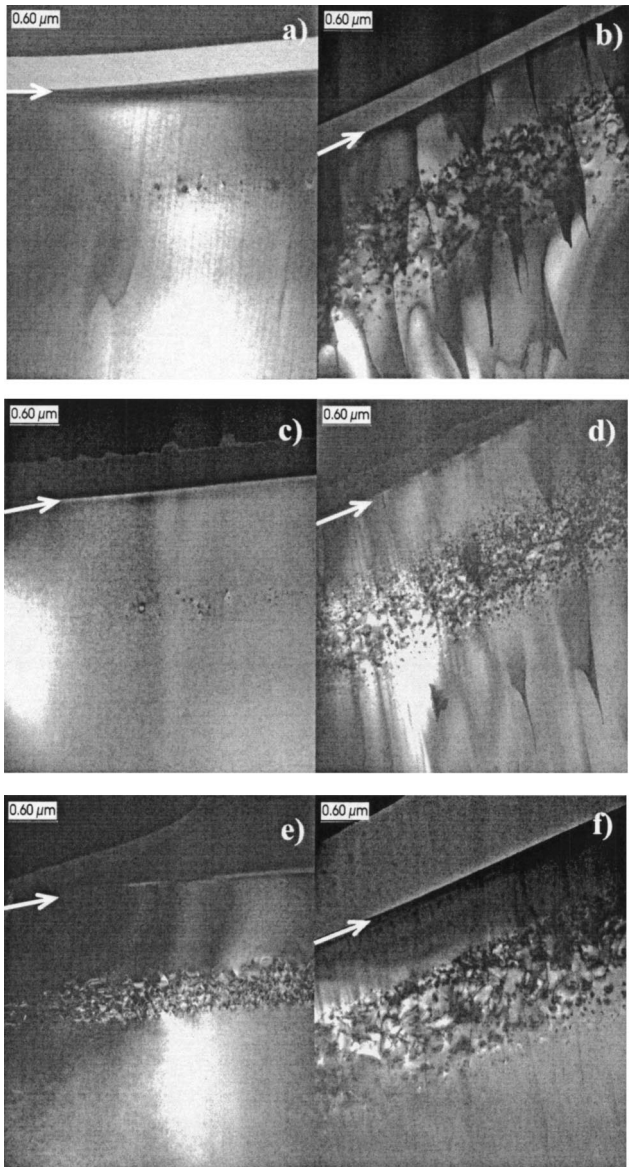

FIG. 3. Cross sectional TEM images of As ion as-implanted (a) and annealed (b), Ga ion as-implanted (c) and annealed (d), and In ion as-implanted (e) and annealed (f) semi-insulating InP. Annealing was for 30 s at 700 °C. Arrow indicates surface.

the form of point defects or small clusters. During the annealing process, agglomeration of these small lattice defects takes place.

Importantly, the type of damage is dependent on implant species: As ion implantation results in a thin layer of loops and clusters which spreads into a thicker layer of larger loops after annealing; Ga ion implantation results in a similarly thin layer of loops and clusters which spreads into a thicker layer of high density loops and clusters after annealing; In implantation results in a thick layer of damage including stacking faults and loops, which spreads into a thicker layer of larger loops and stacking faults after annealing. Thus, it can be seen that the atomic mass of the implant species is not the only factor in determining the degree and type of damage produced in InP, and that the defect accumulation and annihilation mechanisms during the implantation and annealing are different for each implant species.

TABLE I. Effective mobility μ_{eff} sheet carrier concentration N_s, sheet resistance R_s results from Hall effect measurements, and decay time τ from time resolved photoluminescence measurements done on samples implanted with 1 MeV P, 2 MeV As, 2.1 MeV Ga, and 3.3 MeV In ions, to a dose of 10^{16} cm^{-2}, and annealed at 600 and 700 °C for 30 s.

		μ_{eff} (cm^2 V^{-1} s^{-1})	N_s (cm^{-2})	R_s ($\Omega/\square$)	τ (ps)
600 °C	P	2390	1.1×10^{14}	23	5
	Ga	735	3.2×10^{13}	263	0.67
	As	2543	1×10^{14}	24	2.4
	In	2983	1.84×10^{13}	114	1.56
700 °C	P	3250	4.1×10^{14}	48	25
	Ga	2228	4.02×10^{13}	70	3.06
	As	3356	4.3×10^{13}	43	15
	In	3107	5.16×10^{12}	390	3.94

C. Electrical and optical properties

Most of the electrical and optical properties which will be related to the structural data we have presented here are discussed in more detail in other work.[6,7] The main results are summarized in Table I, which shows the electrical and optical characteristics of the samples as measured by the Hall effect and time resolved photoluminescence on these samples, after annealing at 600 and 700 °C. Prior to implantation, a semi-insulating InP wafer has a mobility μ_{eff}, of approximately 2000 cm^2 V^{-1} s^{-1}, sheet carrier concentration N_s of $\sim10^7$ cm^{-2} and sheet resistance R_s of $\sim3\times10^8$ $\Omega/\square$. Implantation into *S-I* InP has been associated with the creation of shallow donors, which decrease the sheet resistance and turn the semiconductor *n*-type; the P-antisite is considered a likely candidate.[7] Implantation with all four ions initially reduced the sheet resistance to $\sim4\times10^5$ $\Omega/\square$, and the electrical properties of the ''as-implanted'' sample, consistent with a material that contains a large number of defects, are not changed significantly by annealing at temperatures below 500 °C. After annealing at 600 °C, the effective mobilities have increased to the unimplanted value of $\sim$2000 cm^2 V^{-1} s^{-1}, the sheet carrier concentrations have peaked in the 10^{13}–10^{14} cm^{-2} range and the sheet resistance has dropped to a minimum of $\sim$20 $\Omega/\square$, with the exception of Ga and In ion implantation. Annealing at 700 °C causes the mobilities to rise $\sim$1.5 times above the unimplanted value to $\sim$3000 cm^2 V^{-1} s^{-1}, again with the exception of Ga ion implantation; R_s stays in the tens or hundreds of $\Omega/\square$, and N_s increases only slightly. Similarly to the DCXRD results, P and As ion implanted samples have practically identical electrical behavior as a function of annealing temperature. Annealing at 600 and 700 °C, for Ga and In ion implantation, yields materials with higher sheet resistances and lower carrier concentrations than for P and As ion implantation.

As far as optical measurements are concerned, for P, As, and In ion implants, there is a trend of decreasing lifetime with increasing ion mass, which would be expected from the known dependence of damage on the mass of the implanted ion. The decay times are larger for rapid thermal annealing (RTA) at 700 °C, as more defects are annealed out and consequently there are fewer trapping centers. Interestingly, implantation with Ga produces the shortest decay times (0.67 ps at RTA 600 °C), even though the mass of this ion is similar to As. The shorter decay time is consistent with the evidence of greater structural damage in the DCXRD spectra at these annealing temperatures, the large concentrations of small clusters observed in the XTEM images, and the corresponding fact that the mobility at the same annealing temperatures does not reach the high values that it does for the other samples. Clearly, implantation with Ga ions has produced defects which have a higher thermal stability and/or act as more efficient carrier traps and scattering centers than does implantation with the other species discussed in this article.

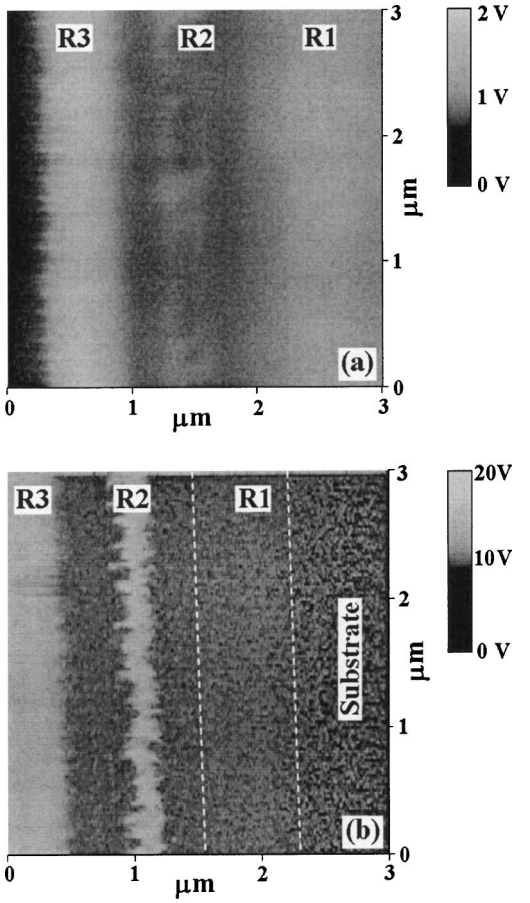

FIG. 4. Ga ion implanted InP annealed at 600 °C: (a) Representative SCM (dC/dV mode) image. The ac and dc biases were, respectively, 2 and 0 V and (b) representative SSRM image. The dc bias was −1 V.

Hall effect measurements have provided an indication of the electrical characteristics corresponding to the path or paths of least resistance in the samples; because these were not multiple-energy implants where the damage profile might be more or less uniform, it is expected that the different layers of damage resulting from the nonuniform damage profile will have different electrical and optical characteristics. It would be useful to know how these characteristics vary as a function of depth into the samples. Such information, at least with regard to the electrical behavior, can be provided by scanning spreading resistance and scanning capacitance microscopy measurements.

Figure 4(a) shows a typical SCM image obtained in the dC/dV-mode for Ga implanted InP annealed at 600 °C. At

this annealing temperature—as was illustrated in the structural measurements of Figs. 1–3—significant defect migration and agglomeration is expected to have occurred in the samples, thus causing highly resistive regions with thicknesses that are different to what is expected for a 2 μm InP epilayer grown on an n^+-InP substrate. In this mode, the SCM signal monotonically increases with decreasing carrier concentration. That is, a brighter contrast corresponds to regions of lower carrier concentration and darker contrast to regions of higher carrier concentration, for example the substrate ($\sim 10^{18}$ cm^{-3}). The contrast band ($R1$) is attributed to the epi/substrate interface region at a depth of ~ 2 μm. The reduced carrier concentration in this region could be due to defects at the interface or migration of defects from the implanted region. The dark band ($R2$), from about 1 to 2 μm, shows a low SCM signal and corresponds to a free carrier concentration value comparable to the substrate. In region $R3$, the bright band followed by a dark region close to the surface is indicative of strongly decreasing carrier concentration.

Figure 4(b) shows a typical image obtained with SSRM for Ga ion implanted InP annealed at 600 °C. The dc bias applied to the sample was -1 V. The contact between the diamond coated tip and InP is known to be Schottky-like, nevertheless, it is possible to relate the sample doping to the measured resistances.[17] Compared to the SCM image, a shift in the features $R1$, $R2$, and $R3$ toward the surface can thus be observed. The substrate appears dark due to low resistance. The contrast at the epi/substrate interface region is not as pronounced as in SCM, but section analysis of the image shows a decreasing carrier concentration. The contrast in region $R2$ consists of a bright narrow band (high resistance) at about 1 μm and dark bands on either side, i.e., a low resistance comparable to the substrate. The location of this narrow band corresponds to the expected location of the implantation peak. Contrast in region $R3$ is indicative of increasing resistance towards the surface, consistent with the SCM image. Thus, the observed inhomogeneity in the electrical properties is qualitatively consistent with XTEM results. Below, we compare the results obtained for the different samples, that is, for different implantation species and different annealing temperatures.

Typical SSRM and SCM results (line scans) obtained on Ga ion implanted InP annealed at different conditions are presented in Figs. 5(a) and 5(b), respectively. Here, we comment that scanning across the sample edge was avoided so as not to have adverse effects on the measurements. The position of the zero of the distance-axis on both Figs. 5(a) and 5(b) does not coincide for all the curves, but the origins are still within a maximum of 200 nm from the edge.

As seen on Figs. 5(a) and 5(b), both SSRM and SCM data show that the epilayer is highly resistive for the sample annealed at 400 °C. In SSRM, one obtains a high resistance, about 10^7 Ω. A small peak is observed approximately 1 μm deep in the epilayer and its location corresponds with the expected maximum implantation depth. Correspondingly for this region, the SCM signal [Fig. 5(b)] is uniformly zero and near 1 μm no special feature could be distinguished. For intrinsic doping levels, due to the very large Debye lengths,

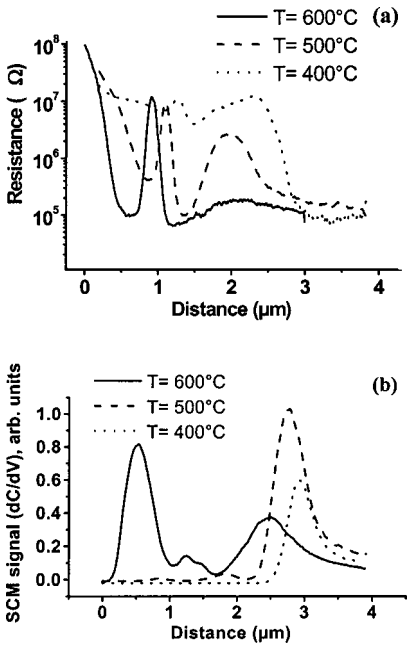

FIG. 5. SSRM and SCM line scans obtained for the Ga ion implanted InP samples annealed at 400, 500, and 600 °C (a) SSRM resistance profiles. (b) SCM profiles (dC/dV mode).

the SCM signal remains close to zero irrespective of the ac bias applied.[13] For the epi-substrate interface region, approximately 2–3 μm, the resistance drops by two orders of magnitude, to the substrate level of about 10^5 Ω. As discussed earlier, the SCM signal shows a peak in this region. For samples with higher annealing temperatures, dramatic changes are observed. As the annealing temperature is increased, one expects annealing of the implantation-induced deep level defects and defect diffusion. The consequences of annealing on the electrical properties in the sample would also depend on the spatial distribution of the defects.

As the annealing temperature is increased (500 and 600 °C), at about 1 μm the SSRM profile still shows a pronounced high-resistance region (peaks in the SSRM profile). The observed location of this peak for the different samples is within 200 nm, which, as mentioned earlier, is within the error in the origin. On either side of this region the resistance is lower and finally in samples annealed at 600 °C it is comparable to that in the substrate. Interestingly, toward the surface the resistance is seen to increase. By contrast, the substrate/epi interface region shows a different behavior: the resistance progressively decreases. The trends seen in the SCM data [Fig. 5(b)] are also consistent with the over-all conclusions obtained from SSRM. Thus, from these measurements it is clear that the recovery of electrical properties after annealing is highly (spatially) non-uniform. In corresponding samples where Hall measurements have been performed, one can conclude that the measured mobilities would correspond primarily to the low resistance regions.

Similar measurements were performed on InP samples implanted with As, P, and In ions. Although the overall features in the SSRM and SCM profiles obtained for the As ion implanted InP are similar to those found for Ga ion implanted samples, the latter case was invariably more resis-

tive. For example, for 600 °C annealing, the resistance in regions framing the maximum implantation peak was much lower in the As ion implanted sample compared to the Ga ion implanted sample; the observed resistances in these regions were nearly one order of magnitude lower than the doped substrate. This is consistent with the higher conductivity in Hall measurements obtained for the As ion case.

In the P ion implanted samples, a high resistance region peak appearing at the 1 μm depth could not be observed. In addition, even at 500 °C annealing, both SCM and SSRM show that most of the epitaxial layer, except close to the surface, is highly conducting. Drastically different results were obtained for the In ion implanted samples. Even at 600 °C, a characteristic zero signal was obtained in the majority of the epilayer in SCM. Correspondingly, SSRM measurements show very high resistances. This appears to be in contradiction to Hall measurements. However, close to the implantation peak, a very low resistance region was observed; its resistance is about five times lower than the substrate level. Such a region would form a highly conducting channel and explains the resistance data obtained in Hall measurements.

These results give detailed information about how the electrical characteristics are locally modified after annealing and how this modification depends on the implanted species. We see that for samples annealed at 400 °C the epilayer is behaving like an insulator. For P ion implantation, annealing at 500 °C creates a conductive layer which occurs at a depth of approximately 1 μm into the sample, and for annealing at higher temperatures this conductive region expands (which is consistent with the broadening of the defective regions after annealing seen in the XTEM scans). For Ga and As ion implantation, annealing at higher temperatures results in intriguing electrical characteristics, in that a double layer of conductivity is formed above and below the 1 μm mark; again for the highest annealing temperature these layers broaden and become more conductive. Given the known shallow donor formation in implanted and annealed InP, it is expected that the highest concentration of these donors would exist in the region of maximum damage. Thus, it makes sense that a layer of high conductivity would be formed at this depth, as is the case for P ion implants. For Ga and As ion implantation, the double conductive layer could be explained as follows: The donors are created in the highest concentration in the region of peak damage, but due to the large amount of scattering and trapping caused by implants with these ions, the mobility and carrier concentration at a depth of 1 μm is very low and thus the paths of least resistance lie above and below the damage peak. For Ga ion implants, the overall resistance of the epilayer remains relatively high and is consistent with the sheet resistances obtained from Hall measurements. In the case of In ion implants, the high resistance regions seen in SSRM (and SCM) in the majority of the epilayer together with a very low resistance (narrow) region close to the implantation peak is once again consistent with the observed trends in Hall data.

IV. CONCLUSION

X-ray and TEM measurements have confirmed a large density of defects after implantation which are arranged in layers, as expected from a nonuniform implant damage profile. The strain profile of these layers is modified by annealing, which allows recrystallization and agglomeration into clusters as well as migration of the original defects. The resulting defect profile is responsible for the optical and electrical properties measured in ion implanted and annealed InP. We have seen how the damage created in the samples depends critically on the implant species, and that Ga ion implantation, with its production of closely spaced small clusters results in unique electrical and optical characteristics.

ACKNOWLEDGMENTS

The Australian Research Council is acknowledged for their financial support. Adam Sikorski is thanked for his assistance with TEM sample preparation. Partial financial support from the Swedish Foundation for International Cooperation in Research and Higher Education (STINT) is acknowledged.

[1] F. W. Smith, A. R. Calawa, C.-L. Chen, M. J. Manfra and L. J. Mahoney, IEEE Electron Device Lett. **9**, 77 (1988).
[2] F. W. Smith, H. Q. Le, V. Diadiuk, M. A. Hollis, A. R. Calawa, S. Gupta, M. Frankel, D. R. Dykaar, G. A. Mourou, and T. Y. Hsiang, Appl. Phys. Lett. **54**, 890 (1989).
[3] S. Gupta, J. F. Whitaker, and G. A. Mourou, IEEE J. Quantum Electron. **28**, 2464 (1992).
[4] M.-J. Tsai and R. H. Bube, J. Appl. Phys. **49**, 3397 (1978).
[5] A. Gasparotto, A. Carnera, C. Frigeri, F. Priolo, B. Fraboni, A. Camporese, and G. Rosetto, J. Appl. Phys. **85**, 753 (1999).
[6] C. Carmody, H. Boudinov, H. H. Tan, C. Jagadish, M. J. Lederer, V. Kolev, B. Luther-Davies, L. V. Dao, and M. Gal, J. Appl. Phys. **92**, 2420 (2002).
[7] C. Carmody, H. H. Tan, C. Jagadish, A. Gaarder, and S. Marcinkevičius, J. Appl. Phys. **94**, 1074 (2003).
[8] S. J. Pearton, C. R. Abernathy, M. B. Panish, R. A. Hamm, and L. M. Lunardi, J. Appl. Phys. **66**, 656 (1989).
[9] H. Boudinov, H. H. Tan, and C. Jagadish, J. Appl. Phys. **89**, 5343 (2001).
[10] S. Ahmed, P. Too, R. Gwilliam, and B. J. Sealy, Appl. Phys. Lett. **79**, 3533 (2001).
[11] A. Gasparotto, A. Carnera, A. Paccagnella, B. Fraboni, F. Priolo, E. Gombia, and R. Mosca, Appl. Phys. Lett. **75**, 668 (1999).
[12] R. C. Barret and C. F. Quate, J. Appl. Phys. **70**, 2725 (1991).
[13] C. C. Williams, Annu. Rev. Mater. Sci. **29**, 471 (1999) and references therein.
[14] S. Anand, IEEE Circuits Devices Mag. **16**, 12 (2000).
[15] P. de Wolf, T. Clarysse, W. Vandervost, L. Hellemans, Ph. Niedermann, and W. Hänni, J. Vac. Sci. Technol. B **16**, 355 (1998).
[16] P. De Wolf, M. Geva, C. L. Reynolds, T. Hantschel, W. Vandervorst, R. B. Bylsma, J. Vac. Sci. Technol. A **17(4)**, 1285 (1999).
[17] R. P. Lu, K. L. Kavanagh, St. J. Dixon-Warren, A. Kuhl, A. J. Spring Thorpe, E. Griswold, G. Hillier, I. Calder, R. Arés, and R. Streater, J. Vac. Sci. Technol. B **19**, 1662 (2001).